Journal of Materials Chemistry C

ROYAL SOCIETY OF CHEMISTRY

PAPER

View Article Online
View Journal | View Issue

Cite this: J. Mater. Chem. C, 2025, 13, 22244

Impact of donor modification on azaisoindigo-based polymers for n- and p-type organic electrochemical transistors

Dilara Gunturkun,[a] Dilara Meli,[bc] Karl J. Thorley,[d] Meike Kuhn,[e] Eva M. Herzig,[e] Jonathan Rivnay[bcf] and Christian B. Nielsen *[a]

Received 11th July 2025,
Accepted 8th October 2025

DOI: 10.1039/d5tc02636a

rsc.li/materials-c

Polymeric organic mixed ionic-electronic conductors have shown remarkable potential as ideal semiconductor materials for organic electrochemical transistors (OECTs), which are emerging as a key technology in next-generation bioelectronics. While numerous conjugated donor–acceptor (D–A) materials based on thiophene, naphthalenediimide, and diketopyrrolopyrrole have been developed, isoindigo counterparts remain comparatively less explored. Herein, we report three D–A polymers based on azaisoindigo (AIG) as the acceptor unit, each containing different donor moieties: bithiophene (2T), difluorinated bithiophene (ff2T), and ethylenedioxy-substituted bithiophene (bisEDOT). By systematically varying the donor strength along the polymer backbone, we switch the dominant charge carrier from p-type with **AIG-bisEDOT** containing the most electron-rich donor moiety to n-type with **AIG-ff2T** incorporating the least electron-rich donor when tested in an OECT device configuration. The underlying structure–property relationships dictating this behaviour are elucidated by means of a joint experimental and computational approach.

1. Introduction

Semiconducting polymers have garnered increasing attention in the development of organic electronic devices, including organic solar cells, organic field-effect transistors, and organic electrochemical transistors (OECTs).[1–7] Recently, significant interest in bioelectronic applications such as neuromorphic computing and electrophysiological measurement has made OECTs a central device platform due to their compatibility for operation in an aqueous environment and high sensing ability.[8–10] Organic mixed ionic-electronic conductors (OMIECs), the active material in the OECT device, enable electronic charge transport through a conjugated polymer backbone while simultaneously facilitating ion transport within the bulk material, typically by means of hydrophilic constituents. Although the combination of poly(3,4-ethylenedioxythiophene) and polystyrene sulfonate (PEDOT:PSS) is the most widely used polymeric OMIEC in the field of bioelectronics, researchers continue to design and develop alternative OMIEC materials to address the drawbacks arising from its inherent doped nature and acidic feature.[11,12]

Designing donor–acceptor (D–A) conjugated polymers serves as an effective way to prepare high-performance OMIECs for several reasons: (1) By modifying the acceptor or donor units, the highest occupied molecular orbital (HOMO) and the lowest unoccupied molecular orbital (LUMO) levels can be judiciously tailored to impart ambient and operational stability and promote efficient charge injection. (2) The introduction of different building blocks or heteroatoms can alter polymer backbone curvature and planarity, often impacting the molecular packing and the microstructure. (3) Various design strategies, such as side-chain engineering, backbone modification, or chemical doping can be easily controlled in these systems.[13–20] Considering these factors, several studies have been reported in the literature focused on optimising the chemical structure and mixed ionic-electronic charge transport properties of D–A type conjugated polymers.[21–26] Recent D–A-based studies have shown that azaisoindigo, also known as diazaisoindigo, is a promising moiety due to its highly electron-deficient nature, coplanar geometry, and ease of chemical modification. Parr *et al.* developed an n-type material, AIG-BT,[27] through copolymerisation with 2,1,3-benzothiadiazole, demonstrating a μC^* (the product of electronic mobility and

[a] Department of Chemistry, Queen Mary University of London, Mile End Road, London E1 4NS, UK. E-mail: c.b.nielsen@qmul.ac.uk
[b] Department of Materials Science and Engineering, Northwestern University, Evanston, Illinois 60208, USA
[c] Northwestern University Materials Research Center, Evanston, Illinois 60208, USA
[d] Center for Applied Energy Research, University of Kentucky, Lexington KY40511, USA
[e] Dynamics and Structure Formation-Herzig Group, University of Bayreuth, Universitätsstraße 30, 95447 Bayreuth, Germany
[f] Department of Biomedical Engineering, Northwestern University, Evanston, Illinois 60208, USA

volumetric capacitance) value of 0.12 F cm^{-1} V^{-1} s^{-1}, while another polymer, gAIID-2FT,[28] achieved a high normalised transconductance value of 0.94 S cm^{-1} in an OECT device, along with excellent operational stability.

When modifying the D–A system, the incorporation of fluorine atoms is a powerful design strategy that is often found to lower the LUMO energy level and enhance intermolecular packing.[29,30] A deeper LUMO energy level has been found to limit electrochemical side-reactions with oxygen and enhance operational stability.[31] Moreover, a recent study demonstrated that incorporation of fluorine atoms can facilitate a switch from p-type to n-type charge transport by modulating charge balance and favouring negative polaron formation.[32] It is particularly noteworthy that manipulating the backbone of the polymers not only alters the microstructure and electrochemical properties but is also effective in the switching mechanism of charge transport.

In this study, we designed and synthesised three azaisoindigo-based D–A conjugated polymers containing different donor moieties, ranging from a strongly electron-donating unit to a much weaker electron-donating motif. We systematically investigated the three polymers' optical, electrochemical, and spectroelectrochemical features in aqueous media as well as their OECT device performances and combined those with structural characterisation to fully understand the structure–property relationships.

2. Results and discussion

2.1. Polymer synthesis and characterisation

The investigated AIG-based polymers are depicted in Scheme 1, whereas the synthetic details of the final dibrominated monomer (AIG) and the polymers are provided in the SI (Scheme S1–S3 and Fig. S1–S6). The AIG monomer contains a five-methylene spacer on its polar amphipathic sidechain synthesised as reported in our previous study.[27] The AIG unit is polymerised *via* traditional Stille coupling polymerisation with commercially available bis-trimethylstannyl-bithiophene and difluoro-bis-trimethylstannyl-bithiophene to afford **AIG-2T** and **AIG-ff2T**, respectively. The polymer **AIG-bisEDOT** is synthesised under direct arylation conditions of dibrominated AIG with 2,2′-bis(3,4-ethylenedioxythiophene) (bisEDOT). The resulting three polymers were subjected to Soxhlet extraction for purification, and finally, the chloroform fraction was collected. All polymers demonstrated moderate solubility in chloroform while remaining insoluble in water, making them well-suited for applications interfacing with an aqueous environment. Their molecular weight analyses were completed by gel permeation chromatography (GPC) using chloroform as the eluent (Fig. S7–S9 and Table S1, SI). The number-average molar mass (M_n) was 47 kDa for **AIG-2T**, 32 kDa for **AIG-ff2T**, and 5 kDa for **AIG-bisEDOT** with all polymers showing broad and bimodal distributions due to aggregation, a common issue for glycolated polymers in the field.[33,34] Limited solubility of **AIG-bisEDOT** in chloroform suggests that GPC is likely to underestimate the molecular weight of this polymer. Therefore, we also used matrix-assisted laser desorption ionisation time-of-flight (MALDI-ToF) mass spectrometry to estimate the molecular weight of all polymers, with peaks in the 6–8 kDa range (Fig. S10–S12, SI), most likely representing the lighter proportion of the actual mass distribution. The thermal properties of the polymers were characterised through thermogravimetric analysis (TGA), and differential scanning calorimetry (DSC) (Fig. S16 and S17, SI). All three polymers exhibited good thermal stability up to 374 °C under nitrogen flow, and their DSC curves indicated no evident thermal transition between 0 and 300 °C.

The optical properties of the polymers were examined in both solution and solid-state with UV-Vis-NIR absorption spectroscopy, as shown in Fig. 1a and b and summarised in Table 1. **AIG-2T** and **AIG-ff2T** polymers exhibit main absorption peaks (at 681 nm and 674 nm, respectively) accompanied by a shoulder (at 747 nm and 740 nm, respectively) in the low-energy band region when measured in solution. In contrast, **AIG-**

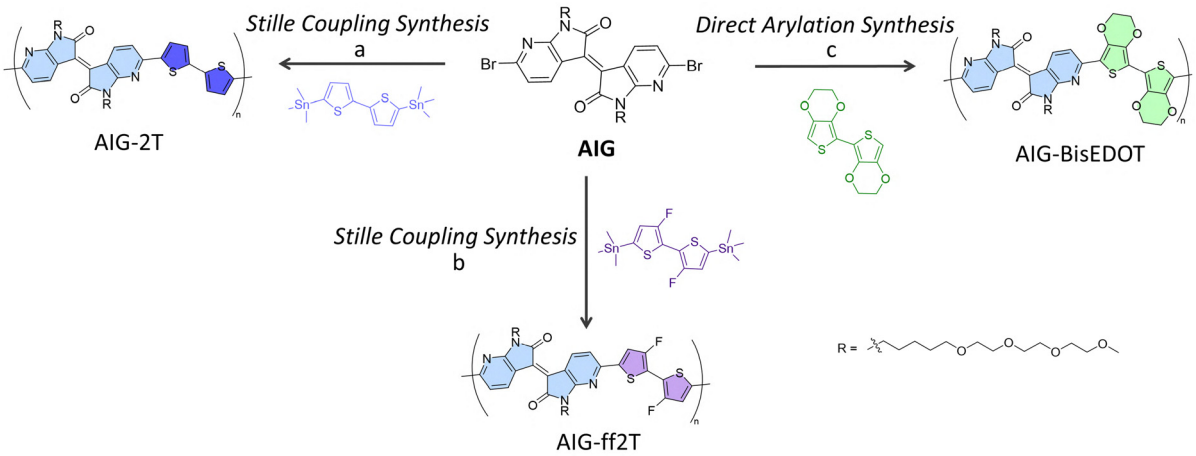

Scheme 1 Synthesis and chemical structures of the azaisoindigo-based polymers with amphipathic sidechains. (a) $Pd_2(dba)_3$, P(*o*-tol)$_3$, 110 °C, Toluene/DMF, 24 h, (b) $Pd_2(dba)_3$, P(*o*-tol)$_3$, 110 °C, Toluene, 24 h, (c) $Pd(OAc)_2$, tris(2-methoxyphenyl)phosphine, Cs_2CO_3, caesium pivalate, 120 °C, chlorobenzene, 30 h.

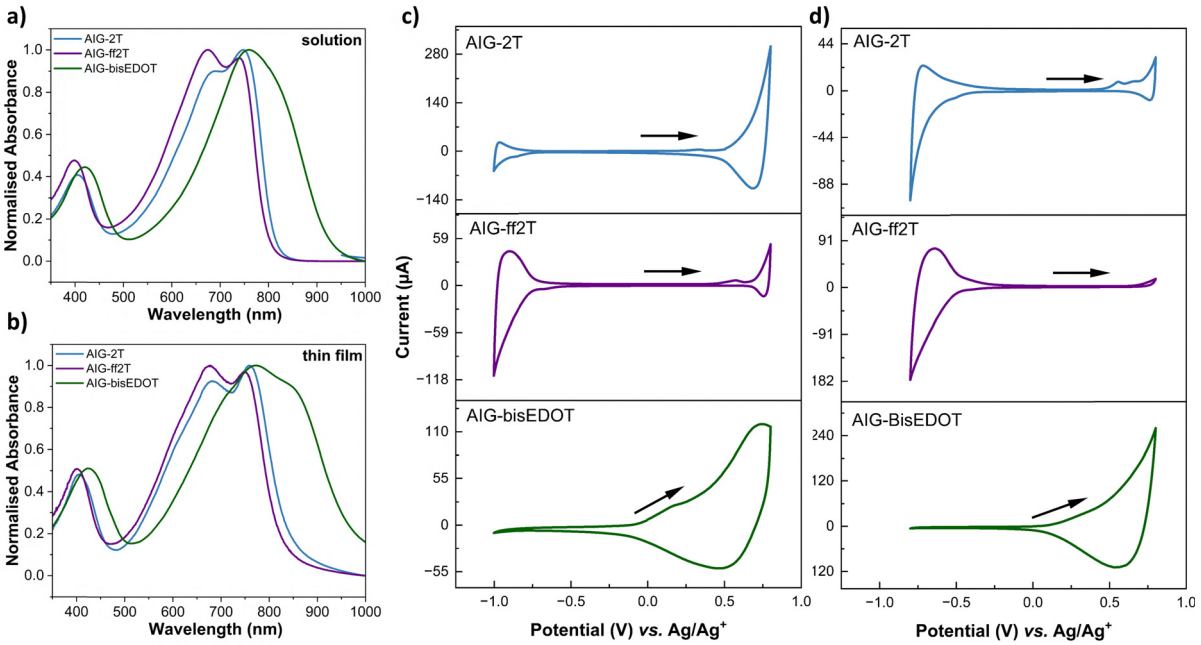

Fig. 1 Normalised UV-Vis-NIR spectra of the polymers in (a) chloroform solution and (b) thin films; cyclic voltammograms of thin films recorded in (c) acetonitrile solution of 0.1 M $TBAPF_6$ at a scan rate of 100 mV s^{-1} and in (d) 0.1 M NaCl aqueous solution at a scan rate of 50 mV s^{-1}.

Table 1 Optical and electrochemical properties of **AIG-2T**, **AIG-ff2T** and **AIG-bisEDOT**

Polymer	$\lambda_{max,solution}$ [a] [nm]	$\lambda_{max,film}$ [b] [nm]	IP [c] [eV]	EA [d] [eV]	E_g^{opte} [eV]	$E_{onset,org}$ [f] [V]	$E_{onset,aq}$ [g] [V]
AIG-2T	681; 747	682; 760	5.25	3.76	1.49	0.58	−0.65 (red)
AIG-ff2T	674; 740	676; 747	5.37	3.85	1.52	0.70	−0.52 (red)
AIG-bisEDOT	761	771; 844	4.93	3.65	1.28	0.26	0.45 (ox)

[a] Measured in chloroform. [b] Measured for polymer films spin-cast from chloroform. [c] IP calculated from the onset of the CV oxidation peak (in organic electrolyte) using the equation IP = $(4.8 - E_{1/2(Fc/Fc+)} + E_{ox})$ eV. [d] EA determined according to equation EA = IP − E_g^{opt}. [e] Calculated from the optical absorption onsets of polymer films using the equation $E_g^{opt} = 1240/\lambda_{onset}$. [f] Determined from the onset of the CV oxidation peak in acetonitrile with 0.1 M $TBAPF_6$. [g] Determined from the onset of the CV reduction or oxidation peak in 0.1 M NaCl aqueous solution.

bisEDOT displays a single absorption band with no vibronic features and an absorption maximum around 760 nm, indicating a more pronounced push–pull effect resulting from the strong donor characteristic of the bisEDOT moiety. In the solid form, as thin films spin-cast from chloroform solution, an obvious shoulder peak appears at 844 nm for **AIG-bisEDOT**, indicative of backbone planarization and aggregation.[35] Thin film spectra for all polymers are red-shifted compared to their solution state, and their absorption maxima are recorded as 682 nm, 676 nm, and 771 nm for **AIG-2T**, **AIG-ff2T**, and **AIG-bisEDOT**, respectively. A decrease in donor strength going from 2 T to ff2T leads to a small blue-shift in the absorption maximum, from 771 nm to 676 nm. The optical band gap of **AIG-bisEDOT** is measured at 1.28 eV, which was calculated from the onset of the solid-state absorption spectrum. This value is notably smaller compared to the optical band gaps of **AIG-2T** and **AIG-ff2T**, which are 1.49 eV and 1.52 eV, respectively. The narrower band gap in **AIG-bisEDOT** could be ascribed to the stronger intermolecular charge transfer between the electron-deficient AIG core and the highly electron-rich bisEDOT unit. As expected, we find that the optical properties and aggregation behaviour of the polymers could be modified by altering the strength of the donor group.

Subsequently, the electrochemical properties of the AIG-based polymers were evaluated using cyclic voltammetry on drop-cast films in both organic (Fig. 1c and Fig. S13, SI) and aqueous electrolyte solutions (Fig. 1d). The onset of oxidation or reduction and corresponding ionisation potential (IP) and electron affinity (EA) values are summarised in Table 1. **AIG-bisEDOT**, which contains the most electron-rich donor unit, exhibited a clear oxidation event with an onset at 0.26 V against Ag/AgCl in 0.1 M tetrabutylammonium hexafluorophosphate solution in acetonitrile with a high current response. However, the reduction behaviour could not be observed within the electrochemical window, as seen in Fig. 1c. **AIG-2T** showed both oxidation and reduction with onsets around 0.58 V and −0.82 V, respectively, in the organic media. On the other hand, the onsets of oxidation and reduction for **AIG-ff2T**, with the weakest electron donor group, are 0.70 V and −0.77 V, respectively. The IP level of **AIG-bisEDOT** reaches the lowest value of

4.93 eV, while **AIG-ff2T** has an IP of 5.37 eV, slightly higher than that of **AIG-2T** (5.25 eV). EA values, which are estimated from the IP and the optical band gap, are 3.76 eV, 3.85 eV, and 3.65 eV for **AIG-2T**, **AIG-ff2T**, and **AIG-bisEDOT**, respectively. EA and IP values, like the optical properties, exhibit a correlation with the strength of the donor group. Notably, fluorination leads to an increase in both IP and EA values, highlighting that backbone engineering serves as an effective way to modulate the electrochemical properties of the conducting polymers. The aqueous electrochemical behaviour follows the same trend observed in organic electrolyte, with notable reduction events for **AIG-2T** and **AIG-ff2T** as well as oxidative behaviour for **AIG-bisEDOT**. The oxidative activity, on the other hand, is markedly lower for **AIG-2T** and **AIG-ff2T** in aqueous electrolyte compared to organic electrolyte.

To understand the electrochemical doping behaviour of the polymer films, we conducted the UV-Vis-NIR measurements in 0.1 M NaCl aqueous solution upon application of negative and positive voltages. When the potential increased from 0 V to 1 V *versus* Ag/AgCl, no changes in the absorption spectra were observed for **AIG-2T** and **AIG-ff2T** (Fig S15a and b, SI) suggesting that the bulk polymer films do not oxidise substantially under these conditions; we ascribe this observation to the relatively high IP values for these two polymers. In contrast, **AIG-bisEDOT** with a significantly lower IP exhibited new absorption peaks at 1050 nm indicating the formation of positive polaron species up to a bias voltage of 0.7 V as depicted in Fig. 2a and b with the spectroelectrochemical onset of oxidation estimated at 0.3 V (Fig. 2c) Meanwhile, the intensity of the intermolecular charge transfer (ICT) absorption peaks (600–950 nm) from the neutral polymer decreased significantly supporting a bulk electrochemical doping effect. During the electrochemical reduction process, spanning the voltage range from 0 to −0.9 V, we observed only very minor shifts in the absorption peaks for **AIG-2T** at a lower potential (<−0.7 V), suggesting poor redox behaviour (Fig. S14, SI). **AIG-ff2T** did not exhibit any significant spectral changes between 0 V and −0.4 V; however, negative polaron absorption peaks at 1020 nm began to appear at voltages lower than −0.6 V while the neutral absorption band showed a substantial bleaching effect (Fig. 2d and e), again indicating bulk electrochemical doping. The spectroelectrochemical onset of reduction was estimated at −0.6 V for **AIG-ff2T**, which is in good agreement with the reduction potential observed in CV (Fig. 2f). No spectroelectrochemical reductive behaviour was observed for **AIG-bisEDOT** (Fig. S15c, SI). Again, we can ascribe these observations to the differences in energetics with **AIG-ff2T** having a higher EA and therefore a more facile reduction process. While **AIG-ff2T** shows facile reductive (n-type) electrochemical doping in an aqueous environment, **AIG-bisEDOT** clearly undergoes oxidative (p-type) doping. These findings indicate that manipulating the backbone of the polymers affects the electrochemical doping characteristics in an aqueous environment and position **AIG-bisEDOT** and **AIG-ff2T** as active OMIEC candidates for p- and n-type OECTs as further explored in the following section.

2.2. OECT device fabrication and characterisation

To investigate the effect of donor functionalisation on the mixed ionic and electronic conduction properties, OECTs were fabricated using **AIG-2T**, **AIG-ff2T**, and **AIG-bisEDOT** as channel materials.

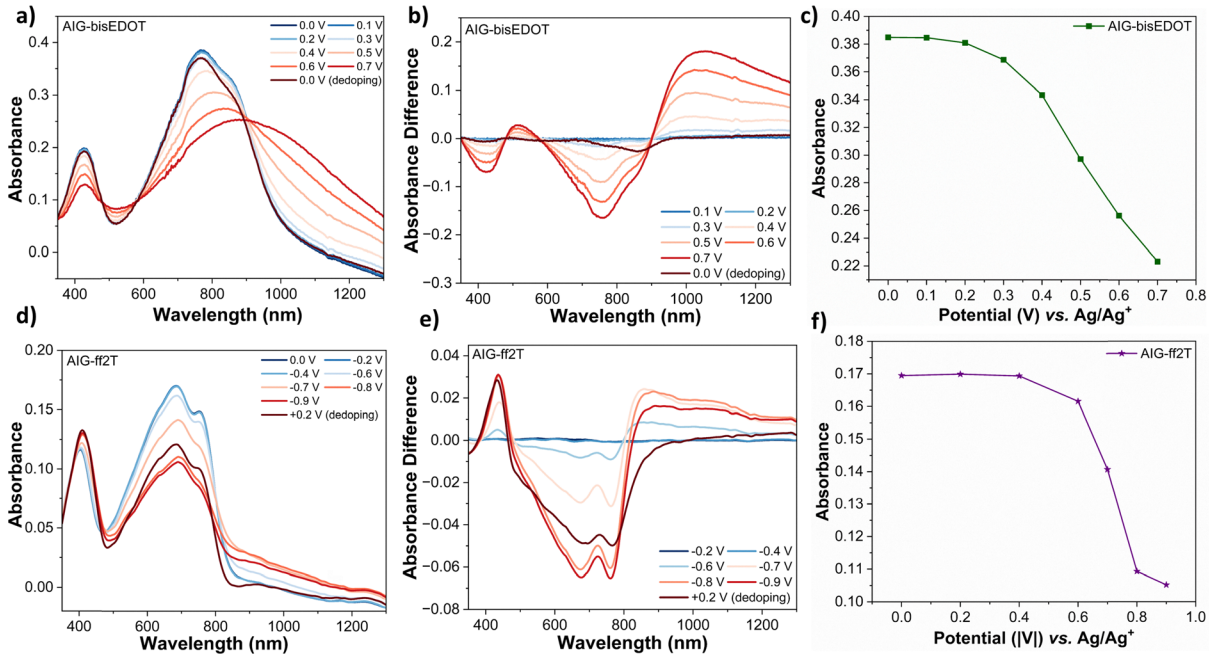

Fig. 2 (a) Spectroelectrochemistry of **AIG-bisEDOT** thin film recorded in 0.1 M aqueous solution, (b) absorbance difference from 0 V spectrum of **AIG-bisEDOT**, (c) bleaching recorded at 770 nm plotted as a function of applied potential for **AIG-bisEDOT**, (d) spectroelectrochemistry of **AIG-ff2T** thin film recorded in 0.1 M aqueous solution, (e) absorbance difference from 0 V spectrum of **AIG-ff2T**, (f) bleaching recorded at 684 nm plotted as a function of applied potential for **AIG-ff2T**.

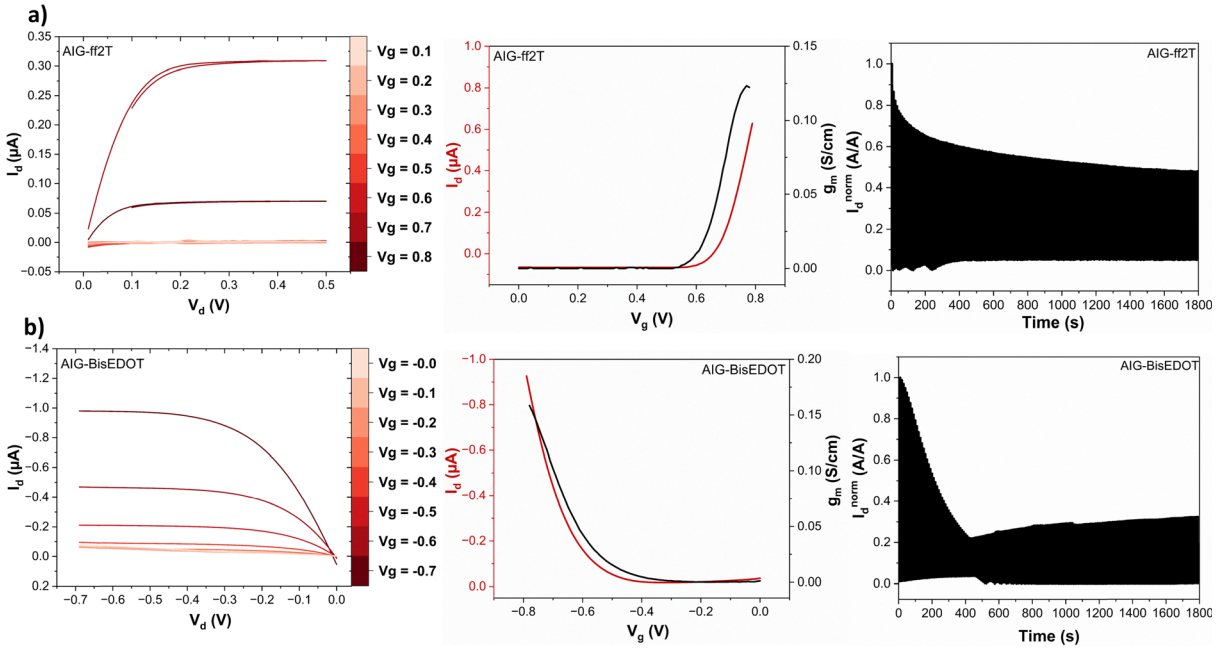

Fig. 3 Output (left), transfer and normalised transconductance (middle), and cycling stability (right) plots for OECTs with (a) **AIG-ff2T**, and (b) **AIG-bisEDOT** active materials at V_d = −0.4 V for p-type (**AIG-bisEDOT**) and V_d = 0.4 V for n-type (**AIG-ff2T**). Transfer and output curves were collected at 0.1 Vs^{-1}.

Polymer solutions were spin-coated onto glass substrates with gold source and drain electrodes and then thermally annealed at 90 °C for 30 min before the devices were tested in a 0.1 M NaCl aqueous solution with an Ag/AgCl electrode as the gate electrode. The detailed fabrication methods have been included in the SI (Section 1). Fig. 3 and Fig. S18 depict the transfer, transconductance, and output curves of the AIG-based polymers, while the characteristic performance parameters of the OECTs are summarised in Table 2. While **AIG-ff2T** functioned as an n-type material with a normalised transconductance (g_m^{norm}) value of 64 mS cm^{-1}, **AIG-2T**, on the other hand, failed to operate as a mixed conductor during the n-type operation in agreement with the spectroelectrochemical data discussed above. Although the **AIG-2T** and **AIG-ff2T**-based devices turned on during p-type operation, strong hysteretic behaviour dissuaded us from ascribing this to bulk oxidative doping effects as also evident from the spectroelectrochemical data. **AIG-bisEDOT** demonstrated p-type OECT operation with a moderate maximum transconductance value of 79 mS cm^{-1}. The threshold voltage (V_{th}) was −0.49 V for **AIG-bisEDOT** (p-type) and around 0.6 V for **AIG-ff2T** (n-type); values which correlate well with the onsets observed during electrochemical (Table 1) and spectroelectrochemical (Fig. 2) analysis of the corresponding polymer films in aqueous media. The OECT figure of merit μC^* was calculated as 0.40 F cm^{-1} V^{-1} s^{-1} and 0.27 F cm^{-1} V^{-1} s^{-1}, respectively, for **AIG-ff2T** (n-type) and **AIG-bisEDOT** (p-type). Next, electrochemical impedance spectroscopy (EIS) was performed to understand the charge storage capability of the polymers (Fig. S19 and S20, SI). **AIG-ff2T** and **AIG-bisEDOT** showed comparable volumetric capacitance C^* values around 96 F cm^{-3}. From the obtained μC^* and C^* values, we calculated the charge carrier mobilities (μ), affording an electron mobility of 0.004 cm^2 V^{-1} s^{-1} for **AIG-ff2T** and a hole mobility of 0.002 cm^2 V^{-1} s^{-1} for **AIG-bisEDOT**. It is worth noting that the electron mobility of the n-type channel material **AIG-ff2T** is comparable to the published azaisoindigo-based n-type OMIECs polymers in literature.[27,28] However, it is also important to consider that the channel widths in the previous literature studies differ from those used herein, which can affect extracted mobility values. During long-term OECT cycling tests, **AIG-bisEDOT** showed limited operational stability, with less than 35% of the original drain current retained after 180 pulses (5 s ON, 5 s OFF) when V_g was varied from 0 to −0.8 V while **AIG-ff2T**

Table 2 Summary of the OECT performance parameters of **AIG-ff2T** and **AIG-bisEDOT** based OECTs

Polymer	d [nm]	OECT operation	V_{th} [a] [V]	$g_{m,max}^{norm}$ [b] [mS cm^{-1}]	C^* [c] [F cm^{-3}]	μ_{OECT} [d] (cm^2 $V^{-1}s^{-1}$)	μC^* [F cm^{-1} V^{-1} s^{-1}]
AIG-ff2T	71 ± 16	n-type	0.61	63.7 ± 33	96.7 ± 2.6	0.004 ± 0.002	0.40 ± 0.28
AIG-bisEDOT	51 ± 30	p-type	−0.49	79.0 ± 30	96.0 ± 0.5	0.002 ± 0.001	0.27 ± 0.13

All the OECT devices were operated in 0.1 M NaCl aqueous solution. [a] Determined by extrapolating the corresponding $I_d^{1/2}$ *vs.* V_g plots. [b] The average transconductance values were normalised by the channel geometry. [c] Extracted from Randles fits of electrochemical impedance spectra. [d] Values extracted from the transistor characteristics in the saturated regime. Average values were extracted from either five or six measured devices. The values indicated after the "±" represent the standard deviation of the data.

showed somewhat better operational stability by varying the V_g from 0 to 0.8 V. (Fig. 3) with around 55% current retention after 180 cycles. In general, the n-type **AIG-ff2T** exhibited better transconductance and μC^* values compared to the widely studied naphthalenediimide-based OMIECs.[15,36] The OECT performance of **AIG-bisEDOT**, meanwhile, lags far behind many p-type OMIECs reported in the literature highlighting azaisoindigo-based polymers' more obvious potential for n-type than for p-type bioelectronic applications.[5,37]

2.3. Computational simulations

Next, density functional theory (DFT) calculations were carried out to probe the electronic properties of the three polymers from a computational viewpoint as further detailed in the SI (Section 3). HOMO and LUMO distributions are shown in Fig. S21 and S22 in SI.

Considering first the electronic properties of the neutral polymer fragments (five repeat units used in calculations), the optimal omega (ω) value represents charge delocalisation along the polymer backbone, with smaller values indicating a higher degree of delocalisation. As seen in Table S2, slightly lower optimal omega values were computed for **AIG-ff2T** and **AIG-bisEDOT** compared to **AIG-2T** indicating inferior charge delocalisation for the 2 T copolymer compared to the other two polymers. Subsequently, considering now the polaronic species, we performed Hirshfeld charge calculations after subdividing the pentameric polymer chain into fragments to study the positive (P^+) and negative (P^-) charge distributions. In positively charged systems, a large fraction of the charge (57–61%) is located on the thiophene-based donor groups as can be seen in Fig. 4. Around 50% of the charge is localised on a single donor moiety for all polymers and spread over the two adjacent AIG units. The similar electronic picture for the positive polarons of the three polymers indicates that the observed differences in OECT device performance are likely ascribed to other factors such as solid-state morphology or charge injection barriers. In contrast to P^+, significant differences are observed when analysing the distribution of negative charges. Firstly, all polymers display a stronger contribution from the electron-deficient AIG segment rather than the donor units in accommodating the negative charge, as could be expected. Interestingly, **AIG-ff2T** demonstrates a greater degree of charge delocalisation along the fragments with the negative charge spread over seven of the ten fragments, and only five in the case of **AIG-2T** and **AIG-bisEDOT**, suggesting higher electron mobility for **AIG-ff2T** than for the other two AIG polymers.

2.4. Film microstructure and characterisation

To investigate the microstructure and molecular packing of the polymer thin films, we carried out two-dimensional grazing-incidence wide-angle X-ray scattering (GIWAXS) (Fig. 5 and Fig. S24, SI) and atomic force microscopy (AFM) studies (Fig. S25, SI). All polymer thin films exhibit distinct scattering patterns, with the lamellar (100) stacking at $q \approx 0.315$–0.374 Å^{-1} and the π–π (010) stacking at $q \approx 1.792$–1.811 Å^{-1}, indicating molecular ordering within the films. However, the extent of this ordering varies between the polymers. **AIG-2T** and **AIG-ff2T** exhibit a well-defined edge-on orientation of the polymer backbone relative to the substrate, with the lamellar stacking in the out-of-plane direction (along q_z) and the π–π stacking in the in-plane direction (along q_r). In contrast, **AIG-bisEDOT** displays more isotropic scattering rings, suggesting

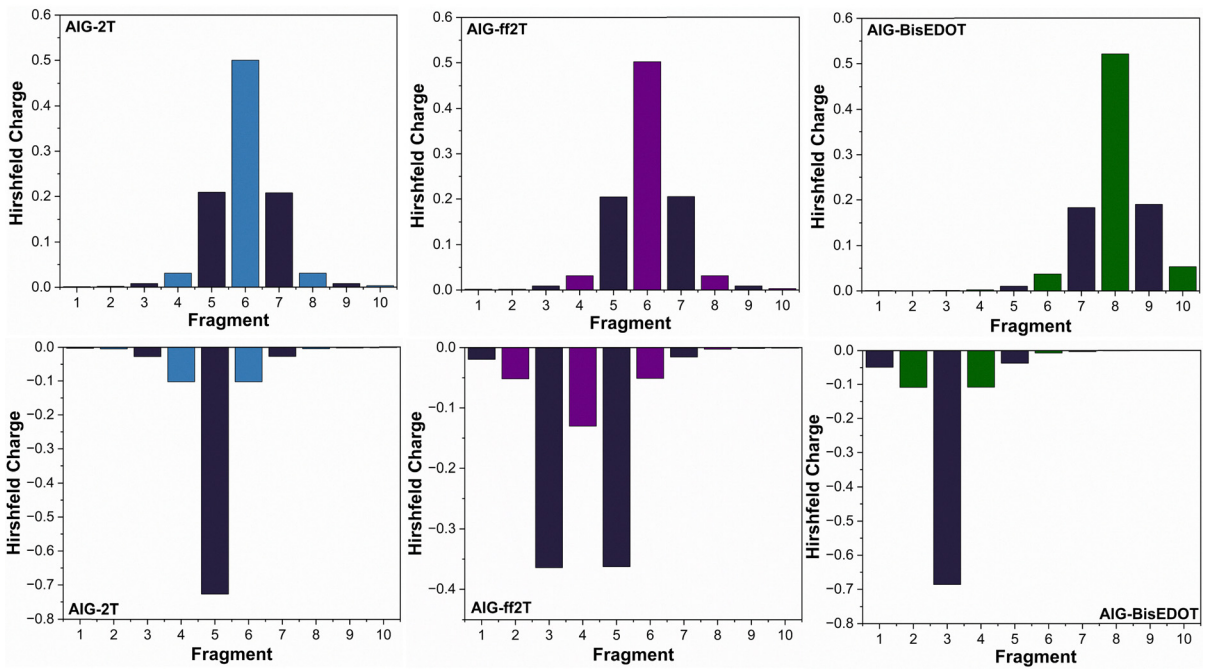

Fig. 4 Hirshfeld charge distribution by fragment (Navy = azaisoindigo; blue = 2T; purple = ff2T; green = bisEDOT) for the polymers. P^+ is shown above and P^- is shown below in the figure.

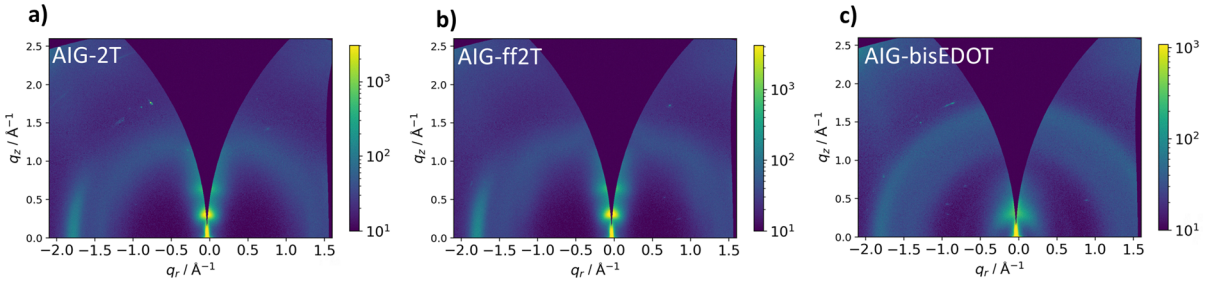

Fig. 5 2D GIWAXS patterns of (a) **AIG-2T**, (b) **AIG-ff2T**, (c) **AIG-bisEDOT** thin films; all films were annealed at 90 °C for 30 min.

less pronounced orientation. For **AIG-bisEDOT**, both lamellar and π–π stacking are observed along q_z and q_r.

As shown in the line-cuts in Fig. 6, **AIG-bisEDOT** exhibits two orders of lamellar (h00) stacking, **AIG-2T** displays three orders, and **AIG-ff2T** exhibits up to four higher-order reflections, indicating an increasing degree of structural long-range order from **AIG-bisEDOT** to **AIG-ff2T**. Moreover, a comparison of the lamellar stacking d-spacings shows a trend from compact to less compact packing going from **AIG-ff2T** (d = (16.78 ± 0.01) Å) to **AIG-2T** (d = (17.02 ± 0.01) Å) and **AIG-bisEDOT** (d = (19.96± 0.39) Å). The increase in d-spacings is accompanied by a decrease of the coherence lengths (L_C) obtained from the widths of the reflections. The coherence lengths decrease from (83.53 ± 0.99) Å for **AIG-ff2T** to (70.77 ± 0.62) Å for **AIG-2T** and to (35.23 ± 0.77) Å for **AIG-bisEDOT**, indicating reduced structural coherence in the lamellar stacking direction for larger d-spacings (Table S3, SI).

For π–π stacking, all polymers exhibit comparable d-spacings between 3.47–3.51 Å, reflecting similar inter-chain distances. However, **AIG-ff2T** again shows the longest coherence length (L_C = 39.54 ± 0.28 Å), followed by **AIG-2T** (L_C = 36.04 ± 0.30 Å) and **AIG-bisEDOT** (L_C = 22.32 ± 0.20 Å), suggesting that **AIG-ff2T** forms the most ordered π–π stacking domains.

Additionally, **AIG-2T** and **AIG-ff2T** exhibit an in-plane peak at q = (1.452 ± 0.004) and (1.487 ± 0.004) Å^{-1}, respectively, marked with □. This peak is attributed to the packing of the oligoethylene glycol helices, in agreement with previous reports.[27,38] In contrast, **AIG-bisEDOT** displays a distinct peak at q = (0.710 ± 0.004) Å^{-1}, marked with Δ, this corresponds to a d-spacing of d = (8.85 ± 0.05) Å. This peak is assigned to cofacial stacking between copolymer backbones as the d-spacing is approximately half the length of the copolymer repeat unit (≈17.07 Å) obtained by DFT calculations, and as observed in similar experimental studies.[27,39] Interestingly, **AIG-bisEDOT** also exhibits a peak at q = (0.486 ± 0.005) Å^{-1}, marked with ▽, which cannot be assigned to a higher order of the lamellar stacking.

From the analysis of both the lamellar and π–π stacking behaviour, it is clear that **AIG-ff2T** has the most ordered microstructure with a tighter lamellar stacking d-spacing than the other polymers and the longest coherence length in both lamellar and π–π stacking direction among the polymer series. **AIG-bisEDOT**, meanwhile, has the least ordered microstructure.

3. Conclusions

In summary, we designed and synthesised a new series of donor–acceptor conjugated polymers containing the azaisoindigo moiety as a strong acceptor unit, combined with 2T, the weak electron-donating group ff2T and the strong electron-donating moiety bisEDOT for OECT applications. By incorporating fluorine atoms into the polymer backbone, both the electron affinity and the ionisation potential increased when

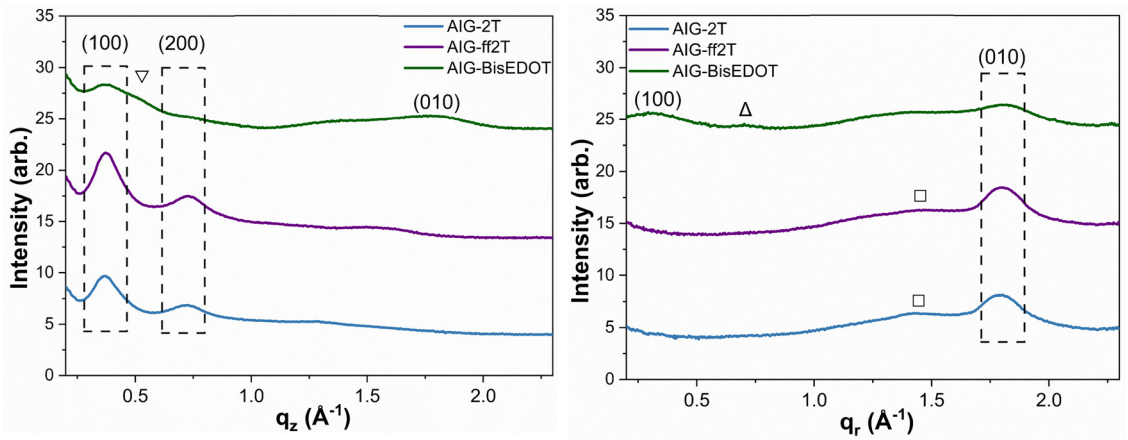

Fig. 6 GIWAXS out-of-plane (q_z) line cuts for **AIG-2T**, **AIG-ff2T**, and **AIG-bisEDOT** and in-plane (q_r) line-cuts for **AIG-2T**, **AIG-ff2T**, and **AIG-bisEDOT** thin films; all films were annealed at 90 °C for 30 min.

comparing **AIG-ff2T** with the non-fluorinated **AIG-2T**. The electron-rich ethylenedioxy moieties of **AIG-bisEDOT** conversely lowered both the electron affinity and the ionisation potential. While **AIG-2T** showed no significant charge modulation in an OECT device, the more electron-rich **AIG-bisEDOT** polymer showed clear p-type behaviour, albeit with a low μC^* value of 0.27 F cm^{-1} V^{-1} s^{-1} ascribed to a low electronic charge carrier mobility which in turn is ascribed to a low degree of structural order in the solid state as confirmed by GIWAXS. In contrast, the electron-deficient **AIG-ff2T** polymer demonstrated clear n-type behaviour, achieving a moderate μC^* value of 0.40 F cm^{-1} V^{-1} s^{-1}, approximately three times higher than what was observed for the previously reported AIG-BT polymer under similar device conditions. **AIG-ff2T** was found to have a reasonable electron mobility of 0.004 cm^2 V^{-1} s^{-1} which was corroborated by a high degree of molecular order as confirmed by GIWAXS measurements and a more delocalised negative polaron as indicated by our computational modelling. The OECT performance of **AIG-bisEDOT** remained limited compared to state-of-the-art p-type polymers, suggesting that azaisoindigo-based polymers are more promising as n-type organic mixed ionic-electronic conductors with room for further improvement through judicious molecular design.

Conflicts of interest

There are no conflicts to declare.

Data availability

The data supporting this article have been included as part of the supplementary information (SI). Supplementary information is available. See DOI: **https://doi.org/10.1039/d5tc02636a**.

Acknowledgements

We would like to thank Lize Bynens for the MALDI-TOF analysis and Martina Rimmele for the GPC analysis. D. M. and J. R. gratefully acknowledge support from the National Science Foundation's Materials Research Science Engineering Center (NSF DMR-2308691). This work made use of the NUFAB facility (RRID:SCR_017779) and the Keck-II facility RRID: SCR_026360) of Northwestern University's NUANCE Center, which has received support from the SHyNE Resource (NSF ECCS-2025633), the IIN, and Northwestern's MRSEC program (NSF DMR-2308691). M. K. and E. M. H. acknowledge the European Innovation Council for funding under the project ICONIC (Grant Agreement 101129638) and Deutsche Forschungsgesellschaft for INST 91/443-1. C. B. N. acknowledges funding from the European Union Horizon Europe under EC Grant Agreement 101129638 and by UK Research and Innovation (UKRI) under the UK government's Horizon Europe funding guarantee [grant number 10104091].

References

1 B. Yin, S. Pang, Z. Chen, W. Deng, Z. Liu, C. Duan, F. Huang and Y. Cao, *Energy Environ. Sci.*, 2022, **15**, 4789–4797.
2 A. Casey, J. P. Green, P. Shakya Tuladhar, M. Kirkus, Y. Han, T. D. Anthopoulos and M. Heeney, *J. Mater. Chem. A*, 2017, **5**, 6465–6470.
3 D. Gunturkun, R. Isci, S. Faraji, B. Sütay, L. A. Majewski and T. Ozturk, *J. Mater. Chem. C*, 2023, **11**, 13129–13141.
4 B. Amna, R. Isci, S. Faraji, H. M. Siddiqi and T. Ozturk, *Org. Electron.*, 2024, **135**, 107147.
5 R. Halaksa, J. H. Kim, K. J. Thorley, P. A. Gilhooly-Finn, H. Ahn, A. Savva, M. Yoon and C. B. Nielsen, *Angew. Chem., Int. Ed.*, 2023, **62**, e202304390.
6 B. D. Paulsen, D. Meli, M. Moser, A. Marks, J. F. Ponder, R. Wu, E. A. Schafer, J. Strzalka, Q. Zhang, I. McCulloch and J. Rivnay, *Chem. Mater.*, 2024, **36**, 1818–1830.
7 Z. S. Parr, R. Halaksa, P. A. Finn, R. B. Rashid, A. Kovalenko, M. Weiter, J. Rivnay, J. Krajčovič and C. B. Nielsen, *ChemPlusChem*, 2019, **84**, 1384.
8 S. Wang, X. Chen, C. Zhao, Y. Kong, B. Lin, Y. Wu, Z. Bi, Z. Xuan, T. Li, Y. Li, W. Zhang, E. Ma, Z. Wang and W. Ma, *Nat. Electron.*, 2023, **6**, 281–291.
9 I. Krauhausen, C.-T. Coen, S. Spolaor, P. Gkoupidenis and Y. van de Burgt, *Adv. Funct. Mater.*, 2024, **34**, 2307729.
10 J. E. Tyrrell, M. G. Boutelle and A. J. Campbell, *Adv. Funct. Mater.*, 2021, **31**, 2007086.
11 J. Cameron and P. J. Skabara, *Mater. Horiz.*, 2020, **7**, 1759–1772.
12 S. T. Keene, T. P. A. van der Pol, D. Zakhidov, C. H. L. Weijtens, R. A. J. Janssen, A. Salleo and Y. van de Burgt, *Adv. Mater.*, 2020, **32**, 2000270.
13 G.-H. Jiang, C.-Y. Li, S.-W. Su and Y.-C. Lin, *J. Mater. Chem. C*, 2024, **12**, 11752–11762.
14 K. Feng, W. Shan, J. Wang, J.-W. Lee, W. Yang, W. Wu, Y. Wang, B. J. Kim, X. Guo and H. Guo, *Adv. Mater.*, 2022, **34**, 2201340.
15 S. Cong, J. Chen, L. Wang, L. Lan, Y. Wang, H. Dai, H. Liao, Y. Zhou, Y. Yu, J. Duan, Z. Li, I. McCulloch and W. Yue, *Adv. Funct. Mater.*, 2022, **32**, 2201821.
16 D. Jeong, I.-Y. Jo, S. Lee, J. H. Kim, Y. Kim, D. Kim, J. R. Reynolds, M.-H. Yoon and B. J. Kim, *Adv. Funct. Mater.*, 2022, **32**, 2111950.
17 K. Guo, J. H. Bai, Y. Jiang, Z. L. Wang, Y. Sui, Y. F. Deng, Y. Han, H. K. Tian and Y. H. Geng, *Adv. Funct. Mater.*, 2018, **28**, 1801097.
18 I.-Y. Jo, D. Jeong, Y. Moon, D. Lee, S. Lee, J.-G. Choi, D. Nam, J. H. Kim, J. Cho, S. Cho, D.-Y. Kim, H. Ahn, B. J. Kim and M.-H. Yoon, *Adv. Mater.*, 2024, **36**, 2307402.
19 W. Yang, K. Feng, S. Ma, B. Liu, Y. Wang, R. Ding, S. Y. Jeong, H. Y. Woo, P. K. L. Chan and X. Guo, *Adv. Mater.*, 2024, **36**, 2305416.
20 X. Zhang, R. Zhu, W. Yang, K. Wang, R. Ding, S. Y. Jeong, H. Y. Woo, K. Feng and X. Guo, *Small*, 2025, **21**, 2408716.
21 S. Heo, J. Kwon, M. Sung, S. Lee, Y. Cho, H. Jung, I. You, C. Yang, J. Lee and Y.-Y. Noh, *ACS Appl. Mater. Interfaces*, 2023, **15**, 1629–1638.

22 B. Ding, I.-Y. Jo, H. Yu, J. H. Kim, A. V. Marsh, E. Gutiérrez-Fernández, N. Ramos, C. L. Rapley, M. Rimmele, Q. He, J. Martín, N. Gasparini, J. Nelson, M.-H. Yoon and M. Heeney, *Chem. Mater.*, 2023, **35**, 3290–3299.
23 X. Luo, H. Shen, K. Perera, D. T. Tran, B. W. Boudouris and J. Mei, *ACS Macro Lett.*, 2021, **10**, 1061–1067.
24 Y. Wang, E. Zeglio, L. Wang, S. Cong, G. Zhu, H. Liao, J. Duan, Y. Zhou, Z. Li, D. Mawad, A. Herland, W. Yue and I. McCulloch, *Adv. Funct. Mater.*, 2022, **32**, 2111439.
25 H. Jia, Z. Huang, P. Li, S. Zhang, Y. Wang, J.-Y. Wang, X. Gu and T. Lei, *J. Mater. Chem. C*, 2021, **9**, 4927–4934.
26 J. Tan, Y. Wang, X. Zhu, J. Duan, R. Liu, C. Chen, C. Ran, Z. Li, B. Ai and W. Yue, *Mater. Chem. Front.*, 2025, **9**, 725–734.
27 Z. S. Parr, J. Borges-González, R. B. Rashid, K. J. Thorley, D. Meli, B. D. Paulsen, J. Strzalka, J. Rivnay and C. B. Nielsen, *Adv. Mater.*, 2022, **34**, 2107829.
28 Y. Wang, G. Zhu, E. Zeglio, T. C. H. Castillo, S. Haseena, M. K. Ravva, S. Cong, J. Chen, L. Lan, Z. Li, A. Herland, I. McCulloch, S. Inal and W. Yue, *Chem. Mater.*, 2023, **35**, 405–415.
29 K. Feng, W. Shan, S. Ma, Z. Wu, J. Chen, H. Guo, B. Liu, J. Wang, B. Li, H. Y. Woo, S. Fabiano, W. Huang and X. Guo, *Angew. Chem., Int. Ed.*, 2021, **60**, 24198.
30 J. Kim, X. Ren, Y. Zhang, D. Fazzi, S. Manikandan, J. W. Andreasen, X. Sun, S. Ursel, H.-I. Un, S. Peralta, M. Xiao, J. Town, A. Marathianos, S. Roesner, T.-T. Bui, S. Ludwigs, H. Sirringhaus and S. Wang, *Adv. Sci.*, 2023, **10**, 2303837.
31 A. Giovannitti, R. B. Rashid, Q. Thiburce, B. D. Paulsen, C. Cendra, K. Thorley, D. Moia, J. T. Mefford, D. Hanifi, D. Weiyuan, M. Moser, A. Salleo, J. Nelson, I. McCulloch and J. Rivnay, *Adv. Mater.*, 2020, **32**, 1908047.
32 P. Li, J. Shi, Y. Lei, Z. Huang and T. Lei, *Nat. Commun.*, 2022, **13**, 5970.
33 L. Bynens, K. Zhang, P. Cavassin, A. Goossens, J. Vanderspikken, T. C. H. Castillo, D. Tsokkou, A. Marks, A. Magni, K. Weaver, L. Lutsen, S. Inal, K. Vandewal, N. Banerji and W. Maes, *Adv. Funct. Mater.*, 2025, 2423913.
34 M. Moser, A. Savva, K. Thorley, B. D. Paulsen, T. C. Hidalgo, D. Ohayon, H. Chen, A. Giovannitti, A. Marks, N. Gasparini, A. Wadsworth, J. Rivnay, S. Inal and I. McCulloch, *Angew. Chem., Int. Ed.*, 2021, **60**, 7777–7785.
35 Y.-Q. Zheng, T. Lei, J.-H. Dou, X. Xia, J.-Y. Wang, C.-J. Liu and J. Pei, *Adv. Mater.*, 2016, **28**, 7213–7219.
36 D. Jeong, I.-Y. Jo, S. Lee, J. H. Kim, Y. Kim, D. Kim, J. R. Reynolds, M.-H. Yoon and B. J. Kim, *Adv. Funct. Mater.*, 2022, **32**, 2111950.
37 C. B. Nielsen, A. Giovannitti, D.-T. Sbircea, E. Bandiello, M. R. Niazi, D. A. Hanifi, M. Sessolo, A. Amassian, G. G. Malliaras, J. Rivnay and I. McCulloch, *J. Am. Chem. Soc.*, 2016, **138**, 10252–10259.
38 R. K. Hallani, B. D. Paulsen, A. J. I. Petty, R. Sheelamanthula, M. Moser, K. J. Thorley, W. Sohn, R. B. Rashid, A. Savva, S. Moro, J. P. Parker, O. Drury, M. Alsufyani, M. Neophytou, J. Kosco, S. Inal, G. Costantini, J. Rivnay and I. McCulloch, *J. Am. Chem. Soc.*, 2021, **143**, 11007–11018.
39 M. Brinkmann, E. Gonthier, S. Bogen, K. Tremel, S. Ludwigs, M. Hufnagel and M. Sommer, *ACS Nano*, 2012, **6**, 10319–10326.

